# Asymmetric Wettability of Nanostructures Directs Leidenfrost Droplets

**Rebecca L. Agapov,[†] Jonathan B. Boreyko,[†] Dayrl P. Briggs,[†] Bernadeta R. Srijanto,[†,‡] Scott T. Retterer,[†] C. Patrick Collier,[†] and Nickolay V. Lavrik[†,*]**

[†]Center for Nanophase Materials Sciences, Oak Ridge National Laboratory, Oak Ridge, Tennessee 37831, United States and [‡]Department of Materials Science and Engineering, University of Tennessee, Knoxville, Tennessee 37996, United States

**ABSTRACT** Leidenfrost phenomena on nano- and microstructured surfaces are of great importance for increasing control over heat transfer in high power density systems utilizing boiling phenomena. They also provide an elegant means to direct droplet motion in a variety of recently emerging fluidic systems. Here, we report the fabrication and characterization of tilted nanopillar arrays (TNPAs) that exhibit directional Leidenfrost water droplets under dynamic conditions, namely on impact with Weber numbers $\geq 40$ at $T \geq 325$ °C. The directionality for these droplets is *opposite* to the direction previously exhibited by macro- and microscale Leidenfrost ratchets where movement *against* the tilt of the ratchet was observed. The batch fabrication of the TNPAs was achieved by glancing-angle anisotropic reactive ion etching of a thermally dewet platinum mask, with mean pillar diameters of 100 nm and heights of 200−500 nm. In contrast to previously implemented macro- and microscopic Leidenfrost ratchets, our TNPAs induce *no* preferential directional movement of Leidenfrost droplets under conditions approaching steady-state film boiling, suggesting that the observed droplet directionality is not a result of the widely accepted mechanism of asymmetric vapor flow. Using high-speed imaging, phase diagrams were constructed for the boiling behavior upon impact for droplets falling onto TNPAs, straight nanopillar arrays, and smooth silicon surfaces. The asymmetric impact and directional trajectory of droplets was exclusive to the TNPAs for impacts corresponding to the transition boiling regime, linking asymmetric surface wettability to preferential directionality of dynamic Leidenfrost droplets on nanostructured surfaces.

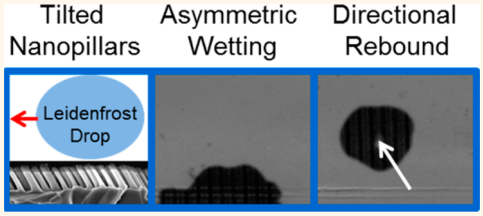


**KEYWORDS:** Leidenfrost · asymmetric wettability · asymmetric rebound · nanopillar · droplet directionality · Weber number · nanostructure

When a droplet is deposited onto a surface heated above a critical temperature, the droplet levitates on a thin cushion of its own vapor.[1] This phenomenon is called the Leidenfrost effect, where droplets exhibit minimal friction and reduced heat transfer from the surface due to the intermediate vapor film.[2] The Leidenfrost regime, also known as film boiling, is in sharp contrast to the nucleate boiling regime where droplets exhibit explosive boiling and maximum heat transfer due to vapor bubble nucleation at the liquid−solid interface.[3] The critical Leidenfrost temperature has previously been found to vary widely depending on the air pressure,[4,5] working fluid,[6] droplet size,[7−9] dynamics of droplet deposition,[10−14] and on the wettability and roughness of the surface.[6,13−22] Enabled by recent advances in microfabrication and nanotechnology, there are now new opportunities in designing micro- or nanostructured surfaces to dramatically increase the Leidenfrost temperature,[16,17,22] which could serve to improve heat transfer at high temperatures.[23,24] Recently, it was discovered that surface roughness can also serve to stabilize vapor layers at temperatures below the Leidenfrost point,[18−21] which could broaden the temperature range for reducing hydrodynamic drag[25] and also have implications in boiling heat transfer systems.

In addition to modifying the Leidenfrost temperature, surface roughness can also control the dynamics of Leidenfrost droplets. Adding crenelations to a surface helps to trap Leidenfrost droplets by increasing their drag by 2 orders of magnitude.[26] When an asymmetric sawtooth structure is utilized, Leidenfrost droplets can even become self-propelled due to the directional

* Address correspondence to lavriknv@ornl.gov.

Received for review October 25, 2013 and accepted December 3, 2013.

**Published online December 03, 2013**
**10.1021/nn405585m**

rectification of their underlying vapor flow.[27] Over the past few years, various mechanisms for the Leidenfrost ratchet have been proposed, including a thermal creep effect driven by an asymmetric temperature profile,[28] a "rocket effect" where the droplet recoils in the opposite direction of vapor flow[29] as a result of momentum conservation, and most commonly, a viscous mechanism where the droplet travels in the same direction as the vapor.[27,30−34] Despite the explosion of interest in modeling the ratchet mechanism, very little work has been done to elucidate the role of ratchet length scale or geometry. Most Leidenfrost ratchets have been fabricated at millimeter length scales,[27,29−32,35] and it remains unclear what effect smaller length scales would achieve besides enabling directional movement of smaller droplet volumes.[33] Furthermore, all ratchets have featured sawtooth geometries, while a much greater variety of periodic shapes, such as overhang structures, tilted grooves, and tilted pillars, can now be fabricated with characteristic sizes from many micrometers down to the nanoscale.

Even for surfaces heated above the Leidenfrost temperature, where droplets appear to be calm and exhibit stable film boiling, it is possible that *partial* liquid−solid contact (known as transition boiling) will intermittently occur.[36] This intermittent transition boiling can be so brief as to prevent any noticeable nucleate boiling, and can be triggered by surface roughness or by impact upon deposition.[36] The curved profile of a Leidenfrost droplet, where the underlying vapor film is thickest in the middle portion of the droplet,[37,38] could also contribute to partial liquid−solid contact at the perimeter of the droplet. The possibility of transition boiling seems especially relevant to Leidenfrost ratchets, which involve asymmetric surface roughness, droplet impact, and continual droplet deformation during translation.[27] Indeed, a recent report found that the ratchet velocity of droplets is significantly increased at lower Leidenfrost temperatures, due to the onset of intermittent transition boiling enhancing droplet transport.[39] It remains a mystery how transition boiling serves to transport droplets, but the partial liquid−solid contact suggests that surface wettability cannot be ruled out.[39] Wettability studies performed at room temperature have demonstrated that asymmetric surfaces exhibiting roughness gradients,[40−42] tilted surface roughness,[43,44] or chemical gradients[45,46] induce directional spreading and rebound of deposited droplets.

Here, we fabricate tilted nanopillar arrays (TNPAs) to demonstrate that intermittent transition boiling induces the directional rebound and movement of Leidenfrost droplets due to the asymmetric wettability of the surface. In contrast to previous Leidenfrost ratchets, our TNPAs do not induce any directionality of Leidenfrost droplets in the steady state. This indicates that the directional movement of deposited droplets is entirely a product of asymmetric wettability of the nanoscale structure upon impact and is not related to vapor flow surrounding the droplets in steady state. Our high-speed video recordings confirm that only bouncing droplets exhibit directionality on TNPAs and that this directional movement is a result of directional rebound. Furthermore, a phase diagram reveals that directional rebound can only occur at temperatures and Weber numbers corresponding to intermittent transition boiling; droplets that exhibited more aggressive liquid−solid contact (nucleate boiling) or no contact (film boiling) were not directional upon impact. It is remarkable that the momentary liquid−solid contact of impacting droplets results in a directional rebound, as the TNPAs are superhydrophilic with droplets irreversibly impaling the nanostructure at room temperature. Our findings reveal that surface wettability strongly influences the dynamic behavior of Leidenfrost droplets, as intermittent liquid−solid contacts occur due to inertial droplet deformation and surface roughness. More broadly, our new fabrication method of glancing-angle anisotropic reactive ion etching will be useful for creating 3D micro- and nanostructures exhibiting tunable wetting, mechanical, and optical properties.

## RESULTS AND DISCUSSION

When a droplet is placed on a periodic nanostructured surface, the droplet shape is symmetric and determined by minimization of total surface energy. The use of channels, grooves,[47−50] or asymmetry[43,44,51] can create local energy barriers that cause the droplet to preferentially spread along one or more axes. Here, novel surfaces in the form of arrays of asymmetric, tilted nanopillars were fabricated to control surface wettability and droplet directionality. The lithography-free fabrication of the tilted nanopillar arrays (TNPAs) made of silicon was achieved by glancing-angle anisotropic reactive ion etching (RIE) of a thermally dewet platinum (Pt) mask,[52−54] with mean pillar diameters of 100 nm and heights of 200−500 nm. The glancing-angle RIE was performed with the sample held at a 70° angle relative to the surface of the carrier wafer and resulted in nanopillars tilted 30° off normal,[55] as shown in Figure 1. The etching angle and the tilt of the resulting nanopillars are not the same due to changes in the electric field caused by the aluminum holder and the sample. For comparison, straight nanopillar arrays (SNPAs) were also fabricated by etching into a silicon wafer positioned horizontally.

The effect of the asymmetric geometry of the TNPA on the liquid spreading behavior was first investigated at room temperature. A deionized water droplet spreads preferentially in the direction of the pillar tilt, with a spreading radius of 1.5:1, as shown in Figure 2.

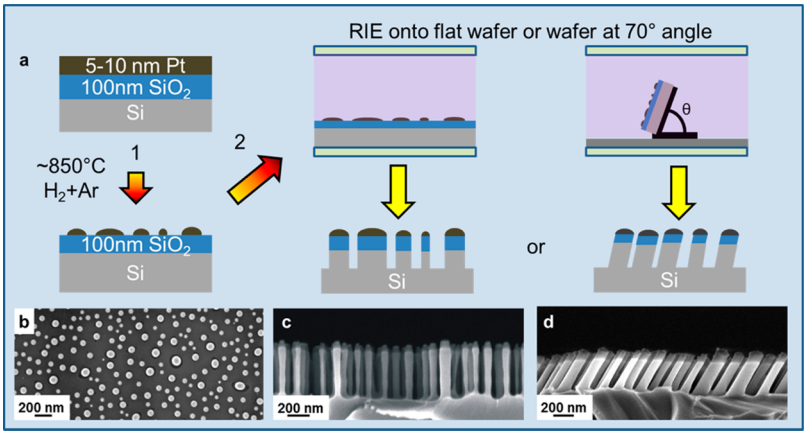


**Figure 1. (a) Fabrication sequence used in the present study to create stochastic nanopillar arrays. A 5 nm layer of Pt was deposited onto a silicon (Si) wafer with 100 nm of thermally grown silicon oxide ($SiO_2$). (a1) Annealing in $H_2$:Ar at ≈850 °C led to the formation of circular Pt islands due to metal dewetting. (a2) RIE etching of a wafer positioned horizontally or a wafer tilted at 70° relative to the carrier wafer resulted in straight or tilted arrays of nanopillars, respectively. (b) SEM image of circular Pt islands formed as a result of dewetting a 5 nm thick Pt film. (c) Cross-sectional SEM image of 500 nm tall straight nanopillar array. (d) Cross-sectional SEM image of 460 nm tall tilted nanopillar array (measured from the substrate along the length of the pillar).**

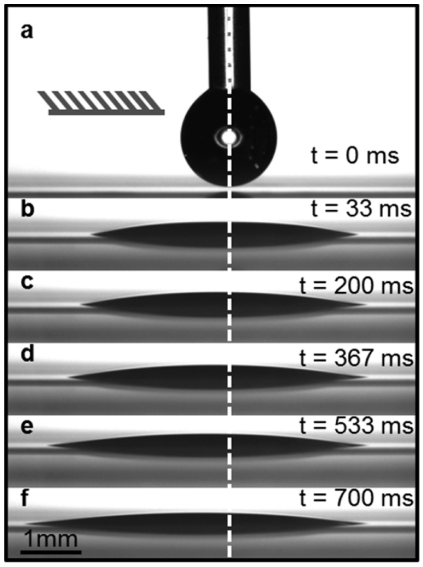


**Figure 2. Spreading of a 2.5 $\mu$L droplet of deionized water on a tilted nanopillar array at the times indicated on the right-hand side of the droplet. The tilt of the pillars is to the left, as shown by the schematic in (a).**

The apparent contact angle of water on the TNPAs is <10°, indicating that the surfaces are superhydrophilic at room temperature.[56,57] The droplets are irreversibly pinned to the nanostructured surface with no observable contraction of the droplet contact line. This preferential wettability of TNPAs is in agreement with previous work[43,58] that found the criterion for spreading is determined by whether the contact line of the droplet can reach the next row of pillars. Chu *et al.*[43] developed a two-dimensional model to explain asymmetric wetting of nanopillar surfaces. In the model, the local contact angle of the liquid, $\theta_{eq}$, which is the intrinsic contact angle measured on a chemically equivalent smooth surface, must be smaller than a critical angle for spreading to occur in a given direction.[59] Bidirectional spreading will occur when $\theta_{eq} < \theta_{eq,-x} < \theta_{eq,+x}$ where $\theta_{eq,-x}$ is the critical spreading angle for spreading against the pillar tilt and $\theta_{eq,+x}$ is the critical spreading angle for spreading in the direction of the pillar tilt. The critical angles are calculated taking into account the height and spacing between the pillars as well as the pillar tilt, relative to normal. In the current case, the average nanopillar height is 300 nm with an average spacing between pillars of 65 nm and tilt of 30° off normal, leading to $\theta_{eq,-x} = 50°$ and $\theta_{eq,+x} = 108°$. When these values are compared to an advancing angle of $\theta_{eq} = 40°$ (±2)° obtained on a smooth reference silicon wafer with native oxide, bidirectional spreading is expected on the TNPAs. However, due to the fact that $\theta_{eq}$ is not significantly lower than $\theta_{eq,-x}$, but much smaller than $\theta_{eq,+x}$, asymmetric spreading occurs preferentially in the direction of the pillar tilt, as shown in Figure 2. For comparison, spreading on a SNPA was bidirectional with a symmetric average spreading radius, as shown in Figure S1 (Supporting Information), and had an apparent contact angle of <10°. The smooth silicon reference with native oxide was hydrophilic with an advancing contact angle of 40° (±2°), a receding contact angle of 22° (±2°), and a contact angle hysteresis of 18° (±4°).

After confirming that the TNPAs induce asymmetric wetting at room temperature, the surface temperature of the nanopillar array was increased to investigate if the asymmetry would lead to directionality for Leidenfrost droplets. Surprisingly, in contrast to previous Leidenfrost ratchets, steady-state Leidenfrost droplets on our TNPAs did not exhibit any directionality. When the droplets were gently placed on the surface of the TNPA, only random motion of the Leidenfrost droplets

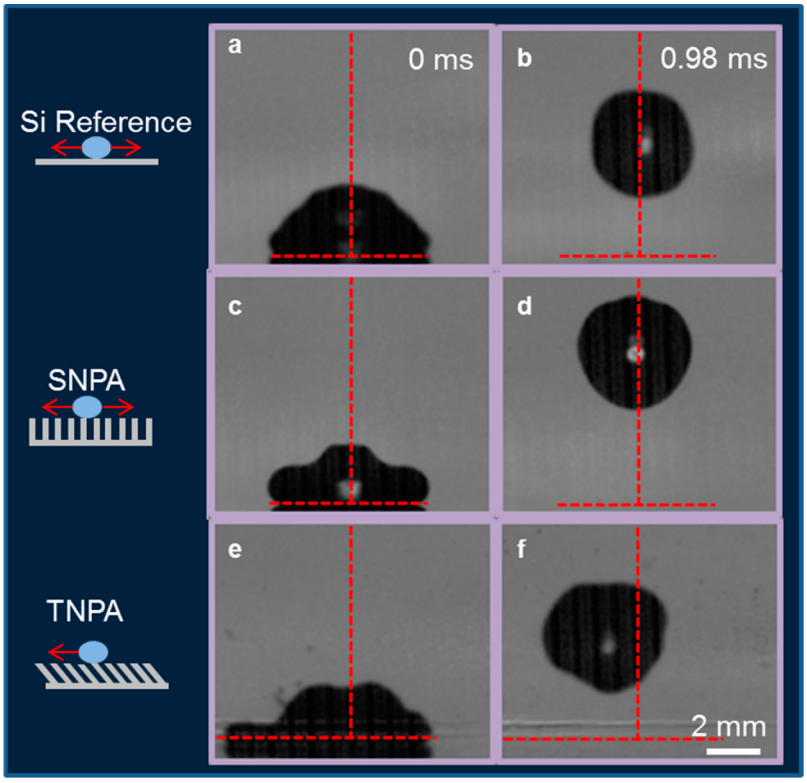


**Figure 3. Representative images of water droplet impact and subsequent rebound at *We* = 360 (impact velocity of ~3 m/s) on a (a and b) smooth Si reference, (c and d) straight nanopillar array (SNPA), and (e and f) tilted nanopillar array (TNPA) at a surface temperature of 350 °C. The dotted lines show the center of mass of the droplet on the substrate surface at drop impact. In all experiments, the TNPAs were oriented with the pillars tilted to the left.**

was observed, as shown in Video V1 (Supporting Information). Therefore, our TNPAs induce no preferential movement of Leidenfrost droplets under conditions approaching steady-state film boiling. There are two possible explanations for this observation. First, the nanoscale pillars are much smaller than the length scale of the vapor film under the droplet, which is on the order of a few micrometers thick when a drop is placed gently on the surface.[12] This difference in length scale may prevent significant rectification of the vapor film under the droplet, leading to no net directionality. Second, the nanopillar arrays are discontinuous whereas traditional Leidenfrost ratchets are continuous in the direction perpendicular to droplet motion. The gaps between the pillars may provide an additional escape path for the vapor flow leading to a nearly isotropic vapor flow through the 3-D pillar array which may affect directional rectification of the vapor.

When the droplets were released onto the surface from a height, directionality was observed with the bouncing droplet moving in the direction of the pillar tilt, as shown in Video V2 (Supporting Information). This is the *opposite* direction compared to traditional sawtooth Leidenfrost ratchets,[29,33,60] but the *same* direction as the asymmetric spreading observed at room temperature. This indicates that surface wettability strongly influences the dynamic behavior of Leidenfrost droplets, as intermittent liquid−solid contacts occur due to inertial droplet deformation and surface roughness. This also suggests that the observed droplet directionality is not a result of asymmetric vapor flow. A high speed camera (1019 frames/s) was used to monitor the droplet impact. Representative images of a droplet impacting the surface and then rebounding on a smooth silicon (Si) wafer, a SNPA, and a TNPA are shown in Figure 3. On the smooth Si reference (Figure 3a,b) and the SNPA (Figure 3c,d), the droplets impact the surface and wet symmetrically. The subsequent droplet rebound is nearly straight up in both of these cases.[12,13,61,62] In contrast, on the TNPA the droplet impacts the surface and wets asymmetrically. The subsequent rebound is directional and coincides with the tilt of the TNPA. This directional rebound is quite remarkable, given the superhydrophilicity of the surface. Rather than completely wetting this superhydrophilic surface upon impact and becoming irreversibly impaled, the droplet *partially* wets the surface[63,64] and then experiences a rebound due to the formation of a vapor film under the droplet due to the Leidenfrost effect. This very brief contact and asymmetric wetting of the TNPAs is sufficient to create a directional rebound and rectify the movement of the droplet, which was previously only observed with hydrophobic surfaces.[40,41,65]

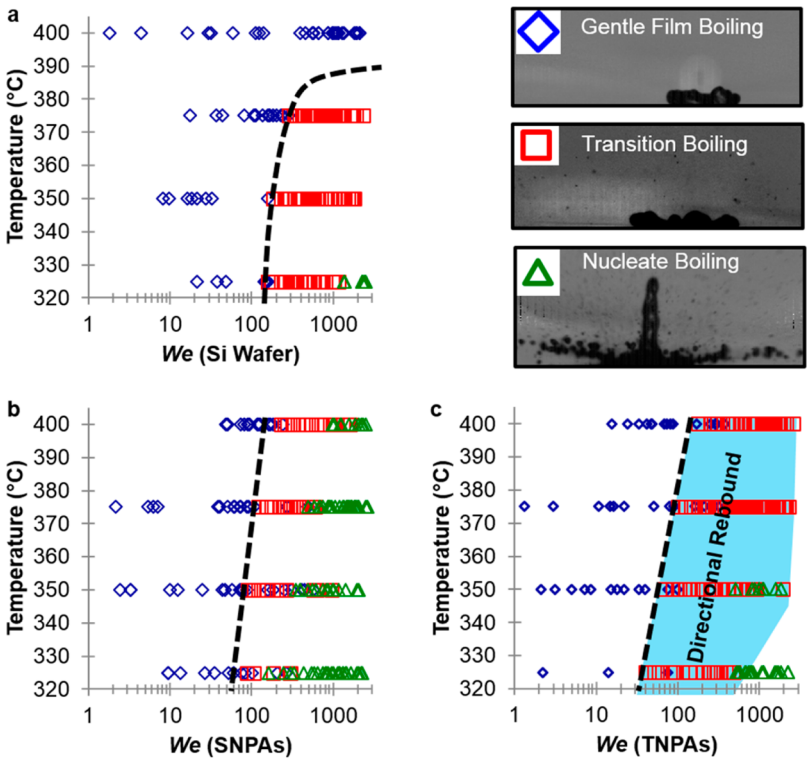


**Figure 4. Phase diagram for droplet impact at different *We* on heated substrates of a (a) smooth Si wafer, (b) straight nanopillar array (SNPA), and (c) tilted nanopillar array (TNPA). The blue diamonds indicate gentle film boiling, the red squares indicate transition boiling where droplet spraying was observed, and the green triangles indicate nucleate boiling where the droplets boiled so quickly that the vapor pressure increased abruptly, causing violent, explosive ejection of tiny droplets due to the venting of vapor bubbles. The dotted black lines are a guide to the eye for the onset of transition boiling. The shaded region in (c) illustrates the transition boiling region where directional rebound is observed after droplet impact onto the TNPAs.**

Due to the necessity of brief contact between the droplet and the surface, a phase diagram was constructed for the TNPAs impacting at different Weber numbers (*We*) to determine under which conditions directionality is achieved. The Weber number compares inertial effects to the surface tension of a droplet:

$$We = \frac{\rho V^2 D}{\sigma} \quad (1)$$

where $\rho$ is the density of the liquid (958 kg/m$^3$ at 100 °C for water), $V$ is its impact velocity, $D$ is the droplet diameter, and $\sigma$ is the surface tension (58 N/m at 100 °C for water). A range of *We* was achieved by changing the drop height and therefore impact velocity of the droplets. The phase diagram is shown in Figure 4. For reference, a phase diagram was constructed for a smooth Si wafer and SNPAs (Figure 4, panels a and b, respectively). On a smooth silicon substrate, the onset of transition boiling occurs at $We \approx 185$ at 350 °C. This shifts to $We \approx 90$ and $We \approx 70$, for SNPAs and TNPAs, respectively, at 350 °C. This decrease in the onset of transition boiling is consistent with other reports indicating that increased surface roughness raises the Leidenfrost temperature relative to a smooth surface.[16,17] This increase of the Leidenfrost temperature relative to a smooth surface would be advantageous for applications where improved heat transfer is required.[23,24] On the TNPAs, a directional rebound occurred for droplets that impacted the surface in the transition boiling regime, where partial liquid–solid contact occurred resulting in mild droplet spraying (Figure 4c). In the gentle film boiling regime, droplets placed on the TNPAs moved randomly, while in the nucleate boiling regime the liquid–solid contact was so violent that the vapor pressure increased abruptly, causing explosive ejection of tiny droplets due to the venting of vapor bubbles. As a result, no accurate trajectory could be determined due to the number of satellite droplets. On the Si wafer and SNPAs, the droplets moved randomly in both the transition boiling and gentle film boiling regimes and broke up into satellite droplets in the nucleate boiling regime.

After the droplet impacts were classified, several *We* were chosen to map out the average horizontal velocities of the rebounding droplets at a constant surface temperature of 350 °C, shown in Figure 5a. For the smooth Si wafer and the SNPAs, individual droplets move with velocities on the order of 100 mm/s. However, their average horizontal velocity calculated for a series of droplets is zero at all *We* for both gentle film

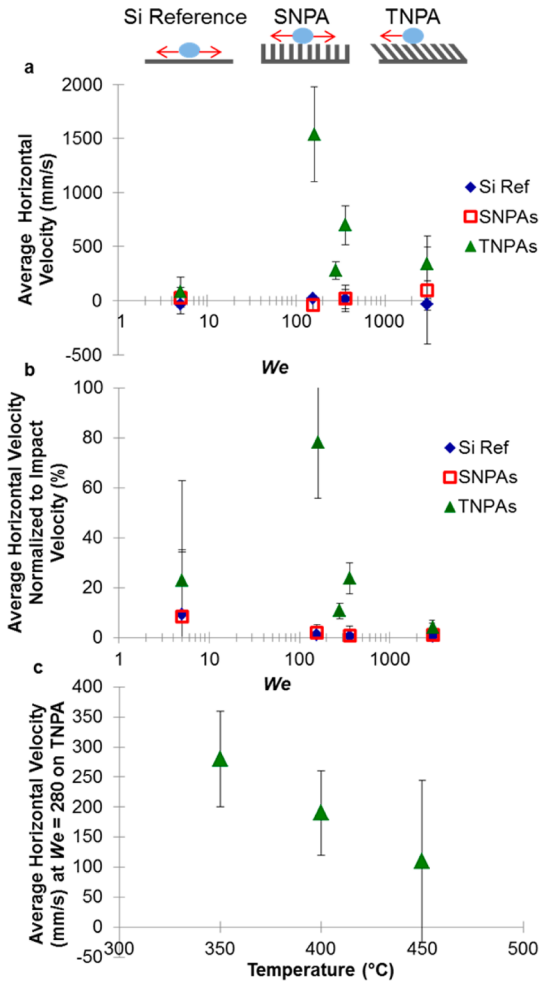


**Figure 5. (a) Average horizontal velocity as a function of *We* on a smooth Si wafer (blue diamonds), SNPAs (red squares), and TNPAs (green triangles) all at a surface temperature of 350 °C. The trajectory for the TNPAs was in the direction of the pillar tilt while the trajectories for the Si reference wafer and the SNPAs were random, as shown in the schematic, averaging to no net horizontal velocity. (b) Average horizontal velocity normalized to impact velocity as a function of *We*. (c) Average horizontal velocity on TNPAs at *We* = 280 as a function of temperature.**

boiling and transition boiling. This is consistent with the symmetry of the underlying surface. Random trajectories are also observed on the TNPAs at *We* < 70 when the droplets are in the gentle film boiling regime. However, droplet movement in the direction of the pillar tilt is observed on TNPAs for 70 < *We* < 3000, *i.e.*, when the droplet is in the transition boiling regime. At *We* ~ 3000, the droplets are in a region between pure transition boiling and total nucleate boiling. This crossover from the transition boiling regime to the nucleate boiling regime is observed in the data as a decrease in the average horizontal velocity. To quantify the strength of the directionality at various *We*, the average horizontal velocities were normalized by the impact velocity, shown in Figure 5b. At *We* = 160 on the TNPA, nearly all of the impact velocity translated into horizontal velocity with a rebound angle of 37° (±6°). At higher *We*, less of the impact velocity was observed as horizontal velocity due to more aggressive spraying with more violent droplet impact and rebound angles of 6° (±4°) at *We* ~ 3000. The velocities reported here are sometimes larger than those reported for micro- and macroscale ratchets, which are typically on the order of 100 mm/s,[27,29,66] but are in agreement with previous work on a nanoscale ratchet[60] where the velocity increased with decreased feature pitch.

To further support the hypothesis that brief contact with the surface is responsible for the directional rebound, the *We* was held constant at *We* = 280 while the temperature was varied from 350 to 450 °C. The average horizontal velocity in the direction of the pillar tilt decreased with increasing temperature, as shown in Figure 5c. This decrease in velocity is due to decreased contact time or extent of contact between the droplet and the surface of the TNPAs at elevated temperatures. Decreased liquid–solid contact time reduces the amount of wetting and therefore the directionality of the rebound. The net directionality decreases when the droplet impact is on the border between the transition boiling regime and the gentle film boiling regime, evident by the data point (with error bars) crossing 0 at 450 °C. At this point, some droplets move against the nanopillar tilt and therefore the overall behavior is less directional than at the same *We* but at a slightly lower temperature when all of the droplets are directional. This demonstrates that altering wettability not only allows for tuning the critical Leidenfrost temperature, but also provides control over heat transfer.

## CONCLUSION

The new potential for asymmetrically nanostructured surfaces to enable a directional rebound effect for droplets in the dynamic Leidenfrost regime has been demonstrated. The lithography-free fabrication of asymmetric TNPAs was achieved by glancing-angle anisotropic reactive ion etching of a thermally dewet platinum mask, with mean pillar diameters of 100 nm and heights of 200–500 nm. The observed directional trajectories of Leidenfrost droplets were exclusive to these asymmetrically nanostructured surfaces and to droplet impacts corresponding to the transition boiling regime. The directionality was completely absent in the case of Leidenfrost droplets in the steady state. This is consistent with the fact that wetting phenomena play no role when there is a stable vapor cushion between the hot surface and the droplets, while intermittent liquid–solid contact may occur during inertial droplet deformation during its impact. Therefore, by contrast to the previously explored macro- and microscale Leidenfrost ratchets, it is the asymmetric wettability

of the resulting nanostructured surfaces that drives the observed directional rebound of droplets in the transition boiling regime. This opens up new opportunities for tunable control of directional fluid flow, varying heat transfer, and modification of the critical Leidenfrost temperature.

## MATERIALS AND METHODS

**Fabrication of Nanopillar Arrays.** A single side polished single crystal Si wafer (100) with 100 nm of thermally grown $SiO_2$ was used as a starting material. A 5 nm thick layer of Pt was deposited onto a Si wafer using physical vapor deposition (PVD) in a vacuum evaporator equipped with an electron gun source (Thermonics Laboratory, VE-240). Wafers with a Pt layer were then thermally processed at ≈850 °C for 8 s in a mixture of argon and hydrogen (10:1) at a pressure of 735 Torr in a cold wall furnace (Easy Tube 3000, First Nano, Ronkonkoma, NY) equipped with a radiative heat source set to its maximum power (22 kW). The resulting dewet Pt layer then served as a mask during anisotropic RIE of the $SiO_2$ and Si.[52−54] The RIE was carried out in an Oxford PlasmaLab system (Oxford Instruments, U.K.) using a combination of inductively coupled plasma and capacitively coupled plasma. The 100 nm of $SiO_2$ was etched in a mixture of $C_4F_8$ and $O_2$ at flow rates of 45 and 2 sccm, respectively, at 15 °C, 7 mTorr for 55 s. The anisotropic etching of Si was carried out at 10 mTorr in a $SF_6$:$C_4F_8$:Ar mixture defined by respective flow rates of 56, 25, and 5 sccm. For the straight nanopillar arrays, etching was performed with the wafer sitting flat in the etching chamber. The TNPAs were fabricated with glancing-angle RIE with the wafer sitting on an aluminum holder bent to an angle of 70° relative to the surface of a silicon carrier wafer. A perfluorinated oil (Fomblin 25/5) was placed between the wafer and the aluminum holder to ensure even heat transfer during etching. Due to the 10 mm clearance height of the load lock in the etcher, a full wafer was diced into 10 mm tall pieces (Disco Abrasive Systems, Automatic Dicing Saw DAD-2H/6) for etching and then reassembled to perform the Leidenfrost experiments. The nanopillar arrays were used "as is" with no additional chemical modification of the surface energy to change the hydrophilicity. The nanopillar dimensions and tilt angle were determined using a scanning electron microscope (Carl Zeiss, Merlin).

**Leidenfrost Experiments.** Droplet impact and motion experiments were conducted on TNPAs, SNPAs, and a single crystal Si wafer (100) with native oxide. These experiments were performed with deionized water on a leveled hot plate and a high speed camera (EPIX X-Cap LTD V3.7, Sun Microsystems, Inc.) to record the droplet trajectory and speed. The temperature was measured with a spot check surface thermometer (PTC Instruments, Model 573C). Droplets of a constant volume (8 $\mu$L) were dispensed with a syringe pump (Harvard Apparatus, Pump II Pico Plus Elite) leading to droplets with diameters of 2.5 mm. The height that the droplet was released from was controlled using a micrometer to alter the needle height connected to the syringe pump. The impact velocity for a droplet was obtained by measuring the vertical distance the droplet traveled between two successive camera frames. Horizontal droplet trajectory and velocity was obtained by analyzing the recorded videos (1019 frames/s) with ImageJ (NIST, Version 1.45r) and monitoring the centroid position in each successive frame. At least 10 droplets were tracked for each surface at each temperature to obtain the average velocities presented. For the phase diagram, the droplets were assigned to a boiling regime based on visual inspection of the impact in the videos.

**Wetting at Room Temperature.** The wetting characteristics at ambient temperature were obtained with a goniometer (Ramé-Hart Instrument Co., Model 590 F4 series with DROPimage Advanced V2.5) recording at 30 frames/s. The spreading of 10 (2.5 $\mu$L) droplets was analyzed to obtain an average on both the SNPAs and TNPAs.

*Conflict of Interest:* The authors declare no competing financial interest.

*Supporting Information Available:* Wetting on a straight nanopillar array and Leidenfrost droplet videos. This material is available free of charge *via* the Internet at http://pubs.acs.org.

*Acknowledgment.* This research was conducted at the Center for Nanophase Materials Sciences, which is sponsored at Oak Ridge National Laboratory by the Division of Scientific User Facilities, U.S. Department of Energy.

## REFERENCES AND NOTES

1. Leidenfrost, J. G. On the Fixation of Water in Diverse Fire. *Int. J. Heat Mass Transfer* **1966**, *9*, 1153–1166.
2. Quéré, D. Leidenfrost Dynamics. *Annu. Rev. Fluid Mech.* **2013**, *45*, 197–215.
3. Nukiyama, S. The Maximum and Minimum Values of the Heat Q Transmitted from Metal to Boiling Water under Atmospheric Pressure. *Int. J. Heat Mass Transfer* **1966**, *9*, 1419–1433.
4. Emmerson, G. S. The Effect of Pressure and Surface Material on the Leidenfrost Point of Discrete Drops of Water. *Int. J. Heat Mass Transfer* **1975**, *18*, 381–386.
5. Celestini, F.; Frisch, T.; Pomeau, Y. Room Temperature Water Leidenfrost Droplets. *Soft Matter* **2013**, *9*, 9535–9538.
6. Bernardin, J. D.; Mudawar, I. The Leidenfrost Point: Experimental Study and Assessment of Existing Models. *J. Heat Transfer* **1999**, *121*, 894–903.
7. Biance, A. L.; Clanet, C.; Quéré, D. Leidenfrost Drops. *Phys. Fluids* **2003**, *15*, 1632–1637.
8. Celestini, F.; Frisch, T.; Pomeau, Y. Take Off of Small Leidenfrost Droplets. *Phys. Rev. Lett.* **2012**, *109*, 034501.
9. Paul, G.; Manna, I.; Das, P. K. Formation, Growth, and Eruption Cycle of Vapor Domes beneath a Liquid Puddle during Leidenfrost Phenomena. *Appl. Phys. Lett.* **2013**, *103*, 084101.
10. Yao, S. C.; Cai, K. Y. The Dynamics and Leidenfrost Temperature of Drops Impacting on a Hot Surface at Small Angles. *Exp. Therm. Fluid Sci.* **1988**, *1*, 363–371.
11. Chandra, S.; Avedisian, C. T. Observations of Droplet Impingement on a Ceramic Porous Surface. *Int. J. Heat Mass Transfer* **1992**, *35*, 2377–2388.
12. Tran, T.; Staat, H. J. J.; Prosperetti, A.; Sun, C.; Lohse, D. Drop Impact on Superheated Surfaces. *Phys. Rev. Lett.* **2012**, *108*, 036101.
13. Tran, T.; Staat, H. J. J.; Susarrey-Arce, A.; Foertsch, T. C.; van Houselt, A.; Gardeniers, H. J. G. E.; Prosperetti, A.; Lohse, D.; Sun, C. Droplet Impact on Superheated Micro-Structured Surfaces. *Soft Matter* **2013**, *9*, 3272–3282.
14. Bernardin, J. D.; Stebbins, C. J.; Mudawar, I. Effects of Suface Roughness on Water Droplet Impact History and Heat Transfer Regimes. *Int. J. Heat Mass Transfer* **1997**, *40*, 73–88.
15. Avedisian, C. T.; Koplik, J. Leidenfrost Boiling of Methanol Droplets on Hot Porous/Ceramic Surfaces. *Int. J. Heat Mass Transfer* **1987**, *30*, 379–393.
16. Kim, H.; Truong, B.; Buongiorno, J.; Hu, L. W. On the Effect of Surface Roughness Height, Wettability, and Nanoporosity on Leidenfrost Phenomena. *Appl. Phys. Lett.* **2011**, *98*, 083121.
17. Kruse, C.; Anderson, T.; Wilson, C.; Zuhlke, C.; Alexander, D.; Gogos, G.; Ndao, S. Extraordinary Shifts of the Leidenfrost Temperature from Multiscale Micro/Nanostructured Surfaces. *Langmuir* **2013**, *29*, 9798–9806.
18. del Cerro, D. A.; Marín, Á. G.; Römer, G. R. B. E.; Pathiraj, B.; Lohse, D.; Huis in't Veld, A. J. Leidenfrost Point Reduction on Micropatterned Metallic Surfaces. *Langmuir* **2012**, *28*, 15106–15110.

19. Vakarelski, I. U.; Patankar, N. A.; Marston, J. O.; Chan, D. Y. C.; Thoroddsen, S. T. Stabilization of Leidenfrost Vapour Layer by Textured Superhydrophobic Surfaces. *Nature* **2012**, *489*, 274–277.
20. Vakarelski, I. U.; Chan, D. Y. C.; Marston, J. O.; Thoroddsen, S. T. Dynamic Air Layer on Textured Superhydrophobic Surfaces. *Langmuir* **2013**, *29*, 11074–11081.
21. Adera, S.; Raj, R.; Enright, R.; Wang, E. N. Non-Wetting Droplets on Hot Superhydrophilic Surfaces. *Nat. Comm* **2013**, *4*, 2518.
22. Kwon, H.; Bird, J. C.; Varanasi, K. K. Increasing Leidenfrost Point Using Micro-Nano Hierarchical Surface Structures. *Appl. Phys. Lett.* **2013**, *103*, 201601.
23. Bernardin, J. D.; Mudawar, I. Experimental and Statistical Investigation of Changes in Surface Roughness Associated with Spray Quenching. *Int. J. Heat Mass Transfer* **1996**, *39*, 2023–2037.
24. Kim, H.; DeWitt, G.; McKrell, T.; Buongiorno, J.; Hu, L. W. On the Quenching of Steel and Zircaloy Spheres in Water-Based Nanofluids with Alumina, Silica, and Diamond Nanoparticles. *Int. J. Multiphase Flow* **2009**, *35*, 427–438.
25. Vakarelski, I. U.; Marston, J. O.; Chan, D. Y. C.; Thoroddsen, S. T. Drag Reduction by Leidenfrost Vapor Layers. *Phys. Rev. Lett.* **2011**, *106*, 214501.
26. Dupeux, G.; Le Merrer, M.; Clanet, C.; Quéré, D. Trapping Leidenfrost Drops with Crenelations. *Phys. Rev. Lett.* **2011**, *107*, 114503.
27. Linke, H.; Aleman, B. J.; Melling, L. D.; Taormina, M. J.; Francis, M. J.; Dow-Hygelund, C. C.; Narayanan, V.; Taylor, R. P.; Stout, A. Self-Propelled Leidenfrost Droplets. *Phys. Rev. Lett.* **2006**, *96*, 154502.
28. Wurger, A. Leidenfrost Gas Ratchets Driven by Thermal Creep. *Phys. Rev. Lett.* **2011**, *107*, 164502.
29. Lagubeau, G.; Le Merrer, M.; Clanet, C.; Quéré, D. Leidenfrost on a Ratchet. *Nat. Phys* **2011**, *7*, 395–398.
30. Dupeux, G.; Le Merrer, M.; Lagubeau, G.; Clanet, C.; Hardt, S.; Quéré, D. Viscous Mechanism for Leidenfrost Propulsion on a Ratchet. *Europhys. Lett.* **2011**, *96*, 58001.
31. Baier, T.; Dupeux, G.; Herbert, S.; Hardt, S.; Quéré, D. Propulsion Mechanisms for Leidenfrost Solids on Ratchets. *Phys. Rev. E* **2013**, *87*, 021001.
32. Dupeux, G.; Baier, T.; Bascot, V.; Hardt, S.; Clanet, C.; Quéré, D. Self-Propelling Uneven Leidenfrost Solids. *Phys. Fluids* **2013**, *25*, 051704.
33. Marín, Á. G.; del Cerro, D. A.; Römer, G. R. B. E.; Pathiraj, B. Huis In't Veld, A. J.; Lohse, D. Capillary Droplets on Leidenfrost Micro-Ratchets. *Phys. Fluids* **2012**, *24*, 122001.
34. Hardt, S.; Tiwari, S.; Baier, T. Thermally Driven Flows Between a Leidenfrost Solid and a Ratchet Surface. *Phys. Rev. E* **2013**, *87*, 063015.
35. Hashmi, A.; Xu, Y.; Coder, B.; Osborne, P. A.; Spafford, J.; Michael, G. E.; Yu, G.; Xu, J. Leidenfrost Levitation: Beyond Droplets. *Sci. Rep.* **2012**, *2*, 797.
36. Bradfield, W. S. Liquid-Solid Contact in Stable Film Boiling. *Ind. Eng. Chem. Fundam.* **1966**, *5*, 200–204.
37. Snoeijer, J. H.; Brunet, P.; Eggers, J. Maximum Size of Drops Levitated by an Air Cushion. *Phys. Rev. E* **2009**, *79*, 036307.
38. Burton, J. C.; Sharpe, A. L.; van der Veen, R. C. A.; Franco, O.; Nagel, S. R. Geometry of the Vapor Layer Under a Leidenfrost Drop. *Phys. Rev. Lett.* **2012**, *109*, 074301.
39. Grounds, A.; Still, R.; Takashina, K. Enhanced Droplet Control by Transition Boiling. *Sci. Rep.* **2012**, *2*, 720.
40. Reyssat, M.; Pardo, F.; Quéré, D. Drops onto Gradients of Texture. *Europhys. Lett.* **2009**, *87*, 36003.
41. Malouin, B. A., Jr.; Koratkar, N. A.; Hirsa, A. H.; Wang, Z. Directed Rebounding of Droplets by Microscale Surface Roughness Gradients. *Appl. Phys. Lett.* **2010**, *96*, 234103.
42. Wu, J.; Ma, R.; Wang, Z.; Yao, S. Do Droplets Always Move Following the Wettability Gradient? *Appl. Phys. Lett.* **2011**, *98*, 204104.
43. Chu, K. H.; Xiao, R.; Wang, E. N. Uni-Directional Liquid Spreading on Asymmetric Nanostructured Surfaces. *Nat. Mater.* **2010**, *9*, 413–417.
44. Malvadkar, N. A.; Hancock, M. J.; Sekeroglu, K.; Dressick, W. J.; Demirel, M. C. An Engineered Anisotropic Nanofilm with Unidirectional Wetting Properties. *Nat. Mater.* **2010**, *9*, 1023–1028.
45. Jokinen, V.; Sainiemi, L.; Franssila, S. Complex Droplets on Chemically Modified Silicon Nanograss. *Adv. Mater.* **2008**, *20*, 3453–3456.
46. Kim, S.; Moon, M. W.; Kim, H. Y. Drop Impact on Super-Wettability-Contrast Annular Patterns. *J. Fluid Mech.* **2013**, *730*, 328–342.
47. Chen, Y.; He, B.; Lee, J.; Patankar, N. A. Anisotropy in the Wetting of Rough Surfaces. *J. Colloid Interface Sci.* **2005**, *281*, 458–464.
48. Chung, J. Y.; Youngblood, J. P.; Stafford, C. M. Anisotropic Wetting on Tunable Micro-Wrinkled Surfaces. *Soft Matter* **2007**, *3*, 1163–1169.
49. Kusumaatmaja, H.; Vrancken, R. J.; Bastiaansen, C. W. M.; Yeomans, J. M. Anisotropic Drop Morphologies on Corrugated Surfaces. *Langmuir* **2008**, *24*, 7299–7308.
50. Seemann, R.; Brinkmann, M.; Karmer, E. J.; Lange, F. F.; Lipowsky, R. Wetting Morphologies at Microstructured Surfaces. *Proc. Natl. Acad. Sci. U.S.A.* **2005**, *102*, 1848–1852.
51. Wu, W.; Cheng, L.; Bai, S.; Wang, Z. L.; Qin, Y. Directional Transport of Polymer Sheet and a Microsphere by a Rationally Aligned Nanowire Array. *Adv. Mater.* **2012**, *24*, 817–823.
52. Strobel, S.; Kirkendall, C.; Chang, J. B.; Berggren, K. K. Sub-10 nm Structures on Silicon by Thermal Dewetting of Platinum. *Nanotechnology* **2010**, *21*, 505301.
53. Lee, J. M.; Kim, B. I. Thermal Dewetting of Pt Thin Film: Etch-Masks for the Fabrication of Semiconductor Nanostructures. *Mater. Sci. Eng., A* **2007**, *449–451*, 769–773.
54. Boreyko, J. B.; Srijanto, B. R.; Nguyen, T. D.; Vega, C.; Fuentes-Cabrera, M.; Collier, C. P. Dynamic Defrosting on Nanostructured Superhydrophobic Surfaces. *Langmuir* **2013**, *29*, 9516–9524.
55. Xu, Z.; Jiang, J.; Gartia, M. R.; Liu, G. L. Monolithic Integrations of Slated Silicon Nanostructures on 3D Microstructures and Their Application to Surface-Enhanced Raman Spectroscopy. *J. Phys. Chem. C* **2012**, 24161–24170.
56. Kim, S. J.; Moon, M. W.; Lee, K. R.; Lee, D. Y.; Chang, Y. S.; Kim, H. Y. Liquid Spreading on Superhydrophilic Micropillar Arrays. *J. Fluid Mech.* **2011**, *680*, 477–487.
57. Seong, J. K.; Kim, J.; Moon, M. W.; Lee, K. R.; Kim, H. Y. Experimental Study of Drop Spreading on Textured Superhydrophilic Surfaces. *Phys. Fluids* **2013**, *25*, 092110.
58. Yang, X. M.; Zhong, Z. W.; Li, E. Q.; Wang, Z. H.; Xu, W.; Thoroddsen, S. T.; Zhang, X. X. Asymmetric Liquid Wetting and Spreading on Surfaces with Slanted Micro-Pillar Arrays. *Soft Matter* **2013**, *9*, 11113–11119.
59. Bico, J.; Tordeux, C.; Quéré, D. Rough Wetting. *Europhys. Lett.* **2001**, *55*, 214–220.
60. Ok, J. T.; Lopez-Ona, E.; Nikitopoulos, D. E.; Wong, H.; Park, S. Propulsion of Droplets on Micro- and Sub-Micron Ratchet Surfaces in the Leidenfrost Temperature Regime. *Microfluid. Nanofluid.* **2011**, *10*, 1045–1054.
61. Antonini, C.; Bernagozzi, I.; Jung, S.; Poulikakos, D.; Marengo, M. Water Drops Dancing on Ice: How Sublimation Leads to Drop Rebound. *Phys. Rev. Lett.* **2013**, *111*, 014501.
62. Biance, A. L.; Chevy, F.; Clanet, C.; Lagubeau, G.; Quéré, D. On the Elasticity of an Inertial Liquid Shock. *J. Fluid Mech.* **2006**, *554*, 47–66.
63. Harvie, D. J. E.; Fletcher, D. F. A Hydrodynamic and Thermodynamic Simulation of Droplet Impacts on Hot Surfaces, Part II: Validation and Applications. *Int. J. Heat Mass Transfer* **2001**, *44*, 2643–2659.
64. Harvie, D. J. E.; Fletcher, D. F. A Hydrodynamic and Thermodynamic Simulation of Droplet Impacts on Hot Surfaces, Part I: Theoretical Model. *Int. J. Heat Mass Transfer* **2001**, *44*, 2633–2642.
65. Vaikuntanathan, V.; Kannan, R.; Sivakumar, D. Impact of Water Drops onto the Junction of a Hydrophobic Texture and a Hydrophilic Smooth Surface. *Colloid Surf., A* **2010**, *369*, 65–74.
66. Feng, R. T.; Zhao, W. J.; Wu, X. D.; Xue, Q. J. Ratchet Composite Thin Film for Low-Temperature Self-Propelled Leidenfrost Droplet. *J. Colloid Interface Sci.* **2012**, *367*, 450–454.